

Characteristic analysis on train-induced vibration responses of rigid-frame RC viaducts

Liangming Sun^{*1,2}, Xingwen He², Toshiro Hayashikawa² and Weiping Xie¹

¹*School of Civil Engineering and Architecture, Wuhan University of Technology, Wuhan 430070, China*

²*Graduate School of Engineering, Hokkaido University, Sapporo 060-8628, Japan*

(Received April 12, 2014, Revised July 22, 2015, Accepted July 31, 2015)

Abstract. A three-dimensional (3D) numerical analysis for the train-bridge interaction (TBI) system is actively developed in this study in order to investigate the vibration characteristics of rigid-frame reinforced concrete (RC) viaducts in both vertical and lateral directions respectively induced by running high-speed trains. An analytical model of the TBI system is established, in which the high-speed train is described by multi-DOFs vibration system and the rigid-frame RC viaduct is modeled with 3D beam elements. The simulated track irregularities are taken as system excitations. The numerical analytical algorithm is established based on the coupled vibration equations of the TBI system and verified through the detailed comparative study between the computation and testing. The vibration responses of the viaducts such as accelerations, displacements, reaction forces of pier bottoms as well as their amplitudes with train speeds are calculated in detail for both vertical and lateral directions, respectively. The frequency characteristics are further clarified through Fourier spectral analysis and 1/3 octave band spectral analysis. This study is intended to provide not only a simulation approach and evaluation tool for the train-induced vibrations upon the rigid-frame RC viaducts, but also instructive information on the vibration mitigation of the high-speed railway.

Keywords: vibration response; rigid-frame RC viaduct; high-speed train; the train-bridge interaction; characteristic analysis

1. Introduction

With the rapid economic and urban development, the high-speed railway is becoming a new trend of railway traffics across the world due to its high speed, comfort, punctuality, safety, less land use and so on, including many countries such as China, France, Germany, Italy, Japan, Korea, Spain, etc. Especially in Japan, the high-speed railway system has been served as a vital role in the national transportation network since Tokaido Shinkansen was the first high-speed railway operated from 1964. Its main lines usually pass directly over densely populated urban areas, where the railway structure mainly comprises the viaducts of RC in the form of a portal rigid frame. The operational speed has been increased from 210 km/h at the beginning to 270 km/h at present. Simultaneously, many more high-speed trains have been put into service and the current number of

*Corresponding author, Ph.D., E-mail: sunliangming@gmail.com

trains is five times greater than that of the initial stage. When the high-speed train is running over a bridge, the bridge is subjected to a huge amount of kinetic energy which can induce serious bridge vibrations (Xia *et al.* 2005, Su *et al.* 2010). They propagate to the ambient ground via footing and pile structures, thereby generating some long-term ground vibrations (Takamiya and Bian 2007, Ju *et al.* 2007, He *et al.* 2010, Yokoyama *et al.* 2011). Therefore, they often produce annoyances to residents alongside and malfunction to vibration-sensitive equipment when passing through developed areas or high-tech industrial areas. This should be considered in the high-speed railway research along with the further development of the high-speed railway system.

Regarding high-speed train-induced bridge vibrations, the dynamic behavior of railway bridges has been a crucial research subject in the bridge design and maintenance since the mid-1960s. Basic theory of the dynamics of railway bridges caused by running trains has been widely developed in the past two decades (Frýba 1996, Yang *et al.* 2004, Kwark *et al.* 2004, Garinei and Risitano 2008, Xia *et al.* 2011, Olmos and Astiz 2013). Analytical models of the coupled TBI system together with experimental validations and engineering applications in high-speed railways have been investigated by Tanabe *et al.* (2003), Yang and Lin (2005), Uno *et al.* (2007), Dinh *et al.* (2009), Martínez-Rodrigo (2010), Guo *et al.* (2012), Xie and Xu (2012), Rezvani *et al.* (2013), Zhai *et al.* (2013a, b), Xia *et al.* (2013) among others. Based on these studies, the vertical and lateral dynamic responses of railway bridges, and the safety and stability of high-speed trains during transit, have been examined and reported. Nevertheless, most of these studies focus on the TBI of simply-supported girder and continuous girder bridges. Few studies have been carried out for the TBI of rigid-frame RC viaducts.

As one of typical bridge infrastructures, the rigid-frame RC viaduct was widely applied in the high-speed railways in Japan. Some studies were carried out based on the field measurement and numerical simulation. For instance, Wakui *et al.* (1995), Kawatani *et al.* (2006) and Su *et al.* (2010) investigated the TBI between high-speed trains and rigid-frame RC viaducts at a certain speed through 3D dynamic analysis. However, Wakui *et al.* (1995) analyzed only the vertical deflection at the second mid-span. Kawatani *et al.* (2006) clarified only vertical accelerations of three points at the hanging part, the top of first pier and third pier; Su *et al.* (2010) investigated only acceleration responses of three directions on top of a certain pier. Takamiya and Bian (2007) mainly focused on studying train-induced ground vibrations around Shinkansen viaducts under moving axle loads. From the above studies, it is clear that the vibration properties of rigid-frame RC viaducts subjected to high-speed train excitations have not been substantially explored, which are different from those of simply-supported girder and continuous girder bridges due to the difference in the bridge configuration. Thus, it is essential to study the TBI characteristics of rigid-frame RC viaducts in detail in order to conduct an accurate prediction on the high-speed train-induced vibration properties as well as provide beneficial instruction to the vibration mitigation and maintenance in the high-speed railway.

To this end, a 3D numerical approach is developed in this study for the TBI system based on the authors' previous work (Kawatani *et al.* 2006, He *et al.* 2010). The purpose is to investigate the vibration characteristics of rigid-frame RC viaducts in both vertical and lateral directions caused by running high-speed trains. The analytical model of TBI system is composed of the high-speed train model with multi-DOFs vibration system for each car and the rigid-frame RC viaduct model with three 24 m length bridge blocks. By applying the simulated track irregularities as the self-excitations for the TBI system, the coupled vibration equations of the TBI system are established and a computer program is developed for numerical simulation. The proposed framework is then applied to analyze the dynamic behaviors of the viaducts including accelerations, displacements,

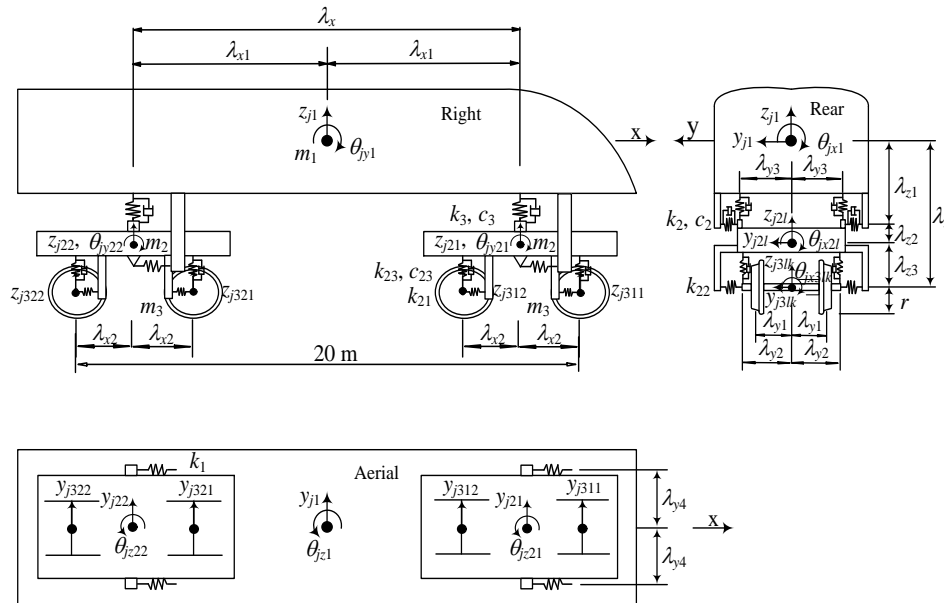


Fig. 1 High-speed train model for vibration analysis

reaction forces of pier bottoms and their amplitudes with train speeds in both vertical and lateral directions. Frequency characteristics are further clarified based on Fourier spectral analysis and 1/3 octave band spectral analysis. Dynamic amplification factors (DAF) of observation points in the down line and up line are also determined.

2. Analytical model of TBI system

The analytical model of the TBI system is composed of three subsystems, namely a high-speed train model, a rail model and a rigid-frame RC viaduct model. The high-speed train model consists of several passenger carriages, and the rigid-frame RC viaduct model consists of multi-span girders, piers and foundations. They are linked by an assumed wheel-rail relationship through the rail model. The simulated track irregularities are considered as the internal self-excitation for the TBI system. In the coordinate system of the TBI system, the longitudinal, lateral and vertical directions are denoted as the x , y and z axes, respectively.

2.1 High-speed train model

The high-speed train model selects 300 Series Shinkansen which is composed of sixteen cars in this analysis based on actual operational conditions. To simplify the analysis and retain its accuracy, the assumption used for the vibration analysis of the TBI system is considered as follows: the high-speed train is running on a straight line at a constant speed, neither accelerating nor decelerating; the wheel-sets remain in full contact with the rail at all times (i.e., no jumps occur) and move with the two rails in both vertical and lateral directions; the uniform high-speed train model is used to describe all of the train carriages without taking into account the differences

between locomotive carriages and normal passenger carriages; the car body, bogies and wheel-sets in each car are regarded as the rigid components, neglecting their elastic deformation during vibration; the connections between the car body, bogies and wheel-sets are represented three-dimensionally by two groups of spring-dashpot suspension devices that are linear springs and viscous dashpots. Each car is treated as a car body, two bogies and four wheel-sets connected by spring-dashpot suspension devices and that is modeled as a complicated multi-DOFs vibration system without the coupling device as shown in Fig. 1. In this model, five DOFs are assigned to each car body or bogie, to account for the lateral motion y_{j1} , bouncing z_{j1} , rolling θ_{jx1} , pitching θ_{jy1} and yawing θ_{jz1} at the center point of the j th car body and the sway motion y_{j2l} , parallel hop z_{j2l} , axle tramp θ_{jx2l} , windup θ_{jy2l} and yawing θ_{jz2l} at the center of gravity of the l th bogie, respectively. For the wheel-set, only three DOFs are considered, which relate to the lateral motion y_{j3lk} , bouncing z_{j3lk} and rolling θ_{jx3lk} . Therefore, it can appropriately reflect vibration responses of the TBI system in both vertical and lateral directions. The vibration properties of the high-speed train are listed in Table 1. The predominant frequencies of the lateral mode and the vertical mode are about 0.805 Hz and 1.073 Hz, respectively.

2.2 Rigid-frame RC viaduct model

The typical RC viaducts in the form of a rigid portal frame for the Japanese high-speed railway are adopted in this study, and their cross section and dimension details are displayed in Fig. 2. The rigid-frame viaducts are built with 24 m length bridge blocks which are separated from each other and connected only by rail structure and ballast at adjacent ends. Each block consists of three 6m length center spans and two 3m length cantilever girders, namely so-called hanging parts, at each end. Three blocks (72m) of the rigid-frame viaducts are adopted for the analysis and modeled with 3D beam elements with six-DOF at each node as shown in Fig. 3. Thus two aspects, connecting

Table 1 Vibration properties of high-speed trains

	Definition	Notation	Value	Definition	Notation	Value	
Mass (t)	car body	m_1	32.818	Damping coefficient (kN·s/m)	upper	c_2	39.2
	bogies	m_2	2.639		lower	c_3	21.6
	wheel-set	m_3	0.9025			c_{23}	19.6
Mass moment of inertia (kN·s ² ·m)		I_{x1}	49.248	Spring constant (kN/m)		k_1	5000.0
	car body	I_{y1}	2512.628		upper	k_2	176.4
		I_{z1}	2512.628			k_3	443.0
	bogies	I_{x2}	2.909		lower	k_{21}	17500.0
		I_{y2}	4.123			k_{22}	4704.0
		I_{z2}	4.123			k_{23}	1209.81
wheel-set	I_{x3}	0.885		λ_x	17.5		
Full length of train /m	L	25	Longitudinal distance /m (Ref. Fig. 1)	λ_{x1}	8.75		
Radius of wheel /m	r	0.43		λ_{x2}	1.25		
Vertical distance /m (Ref. Fig. 1)		λ_z	0.97	Lateral distance /m (Ref. Fig. 1)	λ_{y1}	0.70	
		λ_{z1}	0.50		λ_{y2}	1.00	
		λ_{z2}	0.37		λ_{y3}	1.23	
		λ_{z3}	0.10		λ_{y4}	1.42	

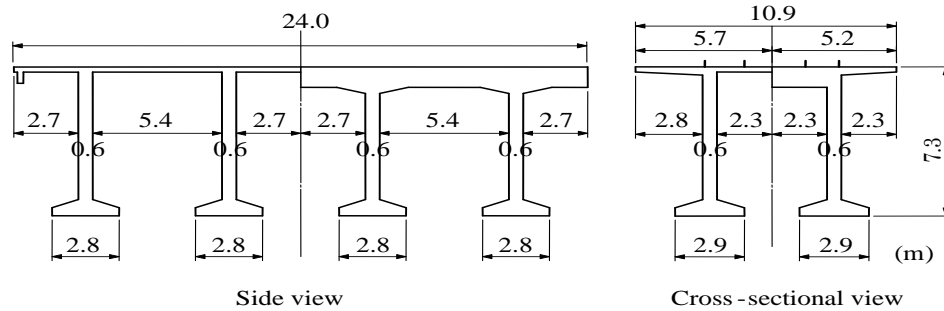


Fig. 2 Dimension of rigid-frame RC viaducts

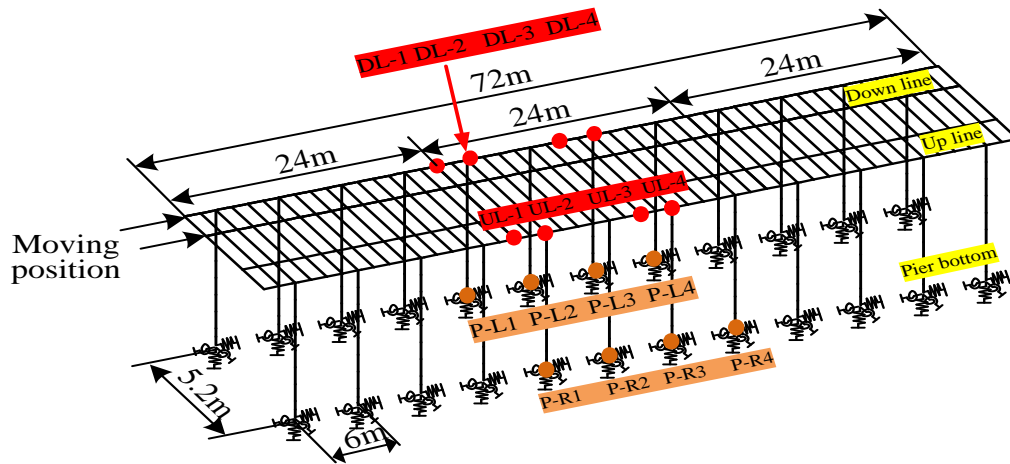


Fig. 3 Rigid-frame RC viaduct model for vibration analysis

effect of the rail structure and the influence of train’s entering and leaving, can be naturally taken into consideration. Only the dynamic responses of the middle block at the observation points of the viaducts indicated in Fig. 3 are examined. The lumped mass system which incorporates the mass of the ballast is utilized for beam elements. The total weight of one block of the viaducts is about 6500kN. Since the high-speed train runs between piers of rigid-frame RC viaducts, the vibration of cantilever slabs in the transverse direction is not important. Therefore, they are not modeled with finite elements to reduce the number of nodes and their masses are added to the outside nodes of the slab. On the other hand, the cantilever slabs in the longitudinal direction of rigid-frame RC viaducts play an important role in the bridge vibration. The bridge slabs are modeled as beam elements with the same length as sleeper intervals, which can express the vibration caused by the rail fastening distance. Double nodes defined as two independent nodes sharing the same coordinate are adopted at the pier bottoms to simulate the effect of ground springs. The ground springs are calculated according to the design codes (RTRI 1997), including the elastic effects of the footing and pile structures as well as the surrounding soil. Listed in Table 2 (Kawatani *et al.* 2006) are the constants of these ground springs. Rayleigh damping assumption is adopted in the structural model and the damping ratio of 3% is adopted for the first and second modes of the structure according to the past field test observations (Nishimura 1990).

Table 2 Ground spring constants

	Pile top			Footing
	Vertical spring	Rotating spring	Lateral spring	Lateral spring
Longitudinal		3.64×10^6 kN·m/rad	8.22×10^4 kN/m	4.84×10^3 kN/m
Transverse	3.86×10^6 kN/m	2.42×10^6 kN·m/rad	8.08×10^4 kN/m	4.72×10^3 kN/m

Table 3 Structural properties of rails

	Mass	Area	Moment of inertia	Spring constant of track
Notation	m_r	A_r	I_r	k_r
Value	60.80 kg/m	77.50 cm ²	3090 cm ⁴	70.00 MN/m

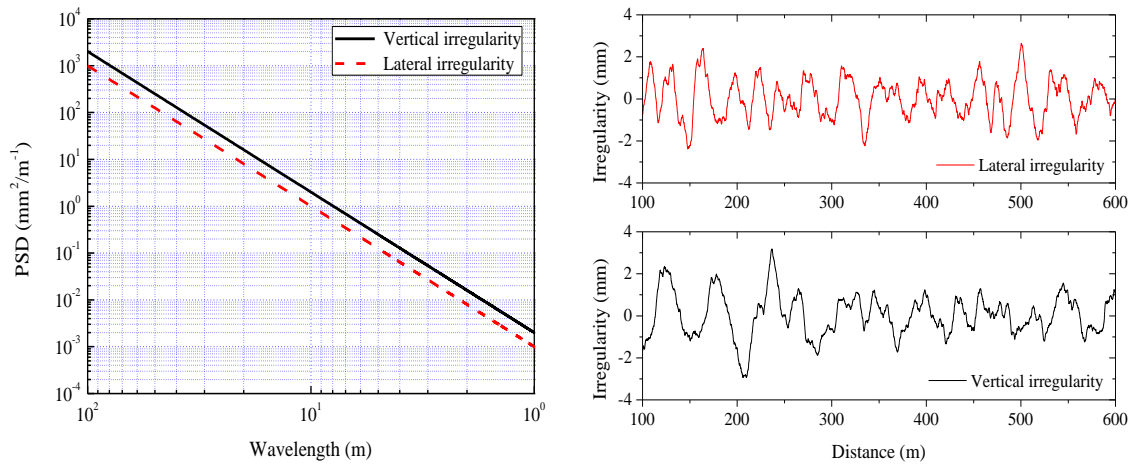


Fig. 4 Track irregularity spectra and simulated profile samples

2.3 Rail model and track irregularity

The rail structure is also modeled as 3D beam elements with six-DOF at each node. Double nodes are also defined here to simulate elastic effects of the sleepers and ballast at the positions of the sleepers. Structural properties of the rails are shown in Table 3. The vertical spring constant of the rail is derived from the ratio of the wheel load to the rail's displacement in the vertical direction. The horizontal spring constant of the rail is assumed to be 1/3 of the value in the vertical direction (Nishimura 1990). Track irregularities of high-speed railways in both vertical and lateral directions are considered in the analysis. Because track irregularities as well as the moving multi-DOFs vibration system of the train are considered to be the most important source of excitation for the vibration analysis of the TBI system. In general, the actual measured track irregularity record is necessary for the specific engineering if a simulation is expected to give a real response result and capture the effect of track irregularities. However, it is not always available for the viaducts considered in a simulation. An alternative approach is to use a power spectral density (PSD) function for the track geometry in the frequency domain to represent the track irregularity. In this study, the PSD functions used for vertical irregularity and lateral irregularity are given in Eqs. (1) and (2), respectively (Matsuura 1998). The samples of track irregularities are simulated based on

the PSD equivalency in the frequency domain (Chen and Zhai 1999). Track irregularity spectra and simulated profile samples used in this study are indicated in Fig. 4.

$$S_v(f) = 2 \times 10^{-9}/f^3 \quad \text{m}^2/(1/\text{m}) \tag{1}$$

$$S_a(f) = 10^{-9}/f^3 \quad \text{m}^2/(1/\text{m}) \tag{2}$$

In which, $f(1/\text{m})$ indicates the spatial frequency of the track irregularity.

3. Analytical method for TBI system

3.1 Vibration differential equations of the high-speed train

3.1.1 Vibration differential equations of the car body

Lateral translation of the car body is given by

$$m_1 \ddot{y}_{j1} - \sum_{l=1}^2 \sum_{m=1}^2 (-1)^m v_{jylm}(t) = 0 \tag{3}$$

Bouncing of the car body can be expressed as

$$m_1 \ddot{z}_{j1} + \sum_{l=1}^2 \sum_{m=1}^2 v_{jzlm}(t) = 0 \tag{4}$$

Rolling of the car body is written by

$$I_{x1} \ddot{\theta}_{jx1} - \sum_{l=1}^2 \sum_{m=1}^2 (-1)^m \lambda_{y3} v_{jzlm}(t) - \sum_{l=1}^2 \sum_{m=1}^2 (-1)^m \lambda_{z1} v_{jylm}(t) = 0 \tag{5}$$

Pitching of the car body is

$$I_{y1} \ddot{\theta}_{jy1} + \sum_{l=1}^2 \sum_{m=1}^2 (-1)^l \lambda_{x1} v_{jzlm}(t) = 0 \tag{6}$$

Yawing of the car body is given by

$$I_{z1} \ddot{\theta}_{jz1} + \sum_{l=1}^2 \sum_{m=1}^2 (-1)^{l+m} \lambda_{x1} v_{jylm}(t) + \sum_{l=1}^2 \sum_{m=1}^2 (-1)^m \lambda_{y4} v_{jxlm}(t) = 0 \tag{7}$$

Where

$$v_{jxlm}(t) = k_1 \{ (-1)^m \lambda_{y4} (\theta_{jz1} - \theta_{jz2l}) \} \tag{8}$$

$$v_{jylm}(t) = k_2 \left\{ \begin{aligned} & -(-1)^m y_{j1} - (-1)^m \lambda_{z1} \theta_{jx1} + (-1)^{l+m} \lambda_{x1} \theta_{jz1} \\ & + (-1)^m y_{j2l} - (-1)^m \lambda_{z2} \theta_{jx2l} \end{aligned} \right\} \\ + c_2 \left\{ \begin{aligned} & -(-1)^m \dot{y}_{j1} - (-1)^m \lambda_{z1} \dot{\theta}_{jx1} + (-1)^{l+m} \lambda_{x1} \dot{\theta}_{jz1} \\ & + (-1)^m \dot{y}_{j2l} - (-1)^m \lambda_{z2} \dot{\theta}_{jx2l} \end{aligned} \right\} \tag{9}$$

$$v_{jzlm}(t) = k_3 \left\{ \begin{aligned} & z_{j1} + (-1)^l \lambda_{x1} \theta_{jy1} - (-1)^m \lambda_{y3} \theta_{jx1} \\ & - z_{j2l} + (-1)^m \lambda_{y3} \theta_{jx2l} \end{aligned} \right\} \\ + c_3 \left\{ \begin{aligned} & \dot{z}_{j1} + (-1)^l \lambda_{x1} \dot{\theta}_{jy1} - (-1)^m \lambda_{y3} \dot{\theta}_{jx1} \\ & - \dot{z}_{j2l} + (-1)^m \lambda_{y3} \dot{\theta}_{jx2l} \end{aligned} \right\} \tag{10}$$

Herein, the subscript j indicates the sequence number of the car. The subscripts relative to the motion of the train body are described as: $l=1, 2$ indicate the front and rear bogies; $m=1, 2$ indicate the left and right sides of the train, respectively. $v_{jxlm}(t)$, $v_{jylm}(t)$ and $v_{jzlm}(t)$, respectively, denote the forces due to the expansion quantities of the upper springs in corresponding directions.

3.1.2 Vibration differential equations of the bogies

Sway of the front or rear bogie is given by

$$m_2 \ddot{y}_{jz1} + \sum_{m=1}^2 (-1)^m v_{jylm}(t) - \sum_{k=1}^2 \sum_{m=1}^2 (-1)^m v_{jylkm}(t) = 0 \quad (11)$$

Parallel hop of the front or rear bogie is expressed as

$$m_2 \ddot{z}_{jz1} - \sum_{m=1}^2 v_{jzlm}(t) + \sum_{k=1}^2 \sum_{m=1}^2 v_{jzlk}(t) = 0 \quad (12)$$

Axle tramp of the front or rear bogie is written by

$$\begin{aligned} I_{x2} \ddot{\theta}_{jx2l} - \sum_{m=1}^2 (-1)^m \lambda_{z2} v_{jylm}(t) + \sum_{m=1}^2 (-1)^m \lambda_{y3} v_{jzlm}(t) \\ - \sum_{k=1}^2 \sum_{m=1}^2 (-1)^m \lambda_{z3} v_{jylkm}(t) - \sum_{k=1}^2 \sum_{m=1}^2 (-1)^m \lambda_{y2} v_{jzlk}(t) = 0 \end{aligned} \quad (13)$$

Windup motion of the front or rear bogie is given by

$$I_{y2} \ddot{\theta}_{jy2l} - \sum_{k=1}^2 \sum_{m=1}^2 (-1)^k \lambda_{z3} v_{jxlm}(t) + \sum_{k=1}^2 \sum_{m=1}^2 (-1)^k \lambda_{x2} v_{jzlk}(t) = 0 \quad (14)$$

Yawing of the front or rear bogie is expressed as

$$\begin{aligned} I_{z2} \ddot{\theta}_{jz2l} - \sum_{m=1}^2 (-1)^m \lambda_{y4} v_{jxlm}(t) + \sum_{k=1}^2 \sum_{m=1}^2 (-1)^{k+m} \lambda_{y2} v_{jxlm}(t) \\ + \sum_{k=1}^2 \sum_{m=1}^2 (-1)^{k+m} \lambda_{x2} v_{jylkm}(t) = 0 \end{aligned} \quad (15)$$

Where

$$v_{jxlm}(t) = k_{21} (-1)^{k+m} \lambda_{y2} \theta_{jz2l} \quad (16)$$

$$v_{jylkm}(t) = k_{22} \{ -(-1)^m y_{jz1} - (-1)^m \lambda_{z3} \theta_{jx2l} + (-1)^{k+m} \lambda_{x2} \theta_{jz2l} + (-1)^m y_{j3lk} \} \quad (17)$$

$$\begin{aligned} v_{jzlk}(t) = k_{23} \{ z_{jz1} - (-1)^m \lambda_{y2} \theta_{jx2l} + (-1)^k \lambda_{x2} \theta_{jy2l} - z_{j3lk} + (-1)^m \lambda_{y2} \theta_{jx3lk} \} \\ + c_{23} \{ \dot{z}_{jz1} - (-1)^m \lambda_{y2} \dot{\theta}_{jx2l} + (-1)^k \lambda_{x2} \dot{\theta}_{jy2l} - \dot{z}_{j3lk} + (-1)^m \lambda_{y2} \dot{\theta}_{jx3lk} \} \end{aligned} \quad (18)$$

Herein, the subscripts relative to the motion of the bogies are described as: $k=1, 2$ indicates the front and rear axles of the bogie, $m=1, 2$ indicate the left and right sides of the bogies, respectively. $v_{jxlm}(t)$, $v_{jylkm}(t)$ and $v_{jzlk}(t)$ denote the forces due to the expansion quantities of the lower springs of relative directions, respectively.

3.1.3 Vibration differential equations of the wheel-sets

Swaying of the wheel-sets is given by

$$m_3 \ddot{y}_{j3lk} + \sum_{m=1}^2 (-1)^m v_{jylkm}(t) = - \sum_{m=1}^2 P_{jylkm}(t) \quad (19)$$

Bouncing of the wheel-sets is expressed as

$$m_3 \ddot{z}_{j3lk} - \sum_{m=1}^2 v_{jzlk}(t) = - \sum_{m=1}^2 P_{jzlk}(t) \quad (20)$$

Rolling of the wheel-sets is written by

$$I_{x3}\ddot{\theta}_{jx3lk} + \sum_{m=1}^2(-1)^m\lambda_{y2}v_{jzlk}(t) = -r\sum_{m=1}^2P_{jylkm}(t) + (-1)^m\lambda_{y1}\sum_{m=1}^2P_{jzlk}(t) \tag{21}$$

Herein, $P_{jylkm}(t)$ and $P_{jzlk}(t)$ respectively represent the dynamic wheel loads acting on the structure in lateral and vertical directions, which are represented as follows

$$P_{jylkm}(t) = -m_3\ddot{w}_{jylkm}/2 - (-1)^mv_{jylkm}(t) \tag{22}$$

$$P_{jzlk}(t) = -(m_1g/8 + m_2g/4 + m_3g/2) - m_3\ddot{w}_{jzlk}/2 + v_{jzlk}(t) \tag{23}$$

Where the variables w_{jylkm} and w_{jzlk} , respectively, denote the sum of the displacements and track irregularities of the rail in the lateral and vertical directions; g is the acceleration of gravity.

3.1.4 Wheel-rail contact relationship

The analytical model of the wheel-rail contact relationship, which links the train movement and the bridge movement, is one of crucial problems to be solved in the TBI system. There are two approaches to deal with the wheel-rail relationship. One is to assume the wheel-rail relationship with rigid contact without considering elastic deformation and the other is to assume the wheel-rail relationship with elastic contact. In this study, the high-speed train model and the rigid-frame viaduct model are dynamically coupled with each other through the rigid contact relationship between the wheels and the rails. Therefore, the relationship between the wheel displacements and the bridge deck displacements can be expressed as

$$y_{j3lk} = \sum_{m=1}^2w_{jylkm}/2 = \sum_{m=1}^2(w_y(t, x_{jlk}) + y_s(x_{jlk}))/2 \tag{24}$$

$$z_{j3lk} = \sum_{m=1}^2w_{jzlk}/2 = \sum_{m=1}^2(w_z(t, x_{jlk}) + z_s(x_{jlk}))/2 \tag{25}$$

$$\theta_{jx3lk} = -(-1)^m\sum_{m=1}^2(w_z(t, x_{jlk}) + z_s(x_{jlk}))/2\lambda_{y1} \tag{26}$$

Where the track irregularities consist of the lateral irregularity $y_s(x_{jlk})$ and vertical irregularity $z_s(x_{jlk})$; x_{jlk} is the coordinate of the m th side of the k th wheel-set of the l th bogie in the j th car along the bridge deck; $w_y(t, x_{jlk})$ and $w_z(t, x_{jlk})$ represent the displacements of the rail at the contact points of the wheel and the rail in y and z -direction, respectively.

$$w_y(t, x_{jlk}) = \Psi_{jylkm}^T(t)\mathbf{w}_b = \{0, \dots, 0, \psi_{p,jlk}, \psi_{p+1,jlk}, 0, \dots, 0\}\mathbf{w}_b \tag{27}$$

$$w_z(t, x_{jlk}) = \Psi_{jzlk}^T(t)\mathbf{w}_b = \{0, \dots, 0, \psi_{q,jlk}, \psi_{q+1,jlk}, 0, \dots, 0\}\mathbf{w}_b \tag{28}$$

Where $\Psi_{jylkm}^T(t)$ and $\Psi_{jzlk}^T(t)$, respectively, denote the interpolation vectors in the lateral and vertical directions in calculating the rail displacement at the contact point from the nodal displacements of the rail element. The transposes of these vectors, as used in Eq. (34), represent the distribution vectors distributing the wheel loads of lateral and vertical directions to the ends of the beam element. The subscripts $p, p+1, q$ and $q+1$ denote the sequence numbers of DOFs in the displacement vector, to which the external force will be distributed. \mathbf{w}_b denotes the nodal displacement vector of the finite element model.

Expanding the equations described above, the differential equations of the high-speed train

model can be expressed in matrix form

$$\mathbf{M}_t \ddot{\mathbf{w}}_t + \mathbf{C}_t \dot{\mathbf{w}}_t + \mathbf{K}_t \mathbf{w}_t = \mathbf{f}_t \quad (29)$$

Where, \mathbf{M}_t , \mathbf{C}_t , \mathbf{K}_t and \mathbf{f}_t , respectively, denote the mass, damping, stiffness matrices and the external force vector of the high-speed train system, which can be derived by expanding those formulae of the high-speed train described above.

3.2 Vibration differential equations of the rigid-frame viaduct

The rigid-frame viaducts with the track structures are modeled as the 3D beam elements. The vibration differential equations of the rigid-frame viaducts can be derived as

$$\mathbf{M}_b \ddot{\mathbf{w}}_b + \mathbf{C}_b \dot{\mathbf{w}}_b + \mathbf{K}_b \mathbf{w}_b = \mathbf{f}_b \quad (30)$$

In which, \mathbf{M}_b , \mathbf{C}_b and \mathbf{K}_b are the mass, damping and stiffness matrices of the bridge system respectively. The lumped mass matrix for the finite elements is adopted in this analysis. The Rayleigh damping is used and the damping matrix \mathbf{C}_b is assumed to be the linear combination between mass and stiffness matrices (Chen *et al.* 2007)

$$\mathbf{C}_b = p_1 \mathbf{M}_b + p_2 \mathbf{K}_b \quad (31)$$

$$p_1 = 2\omega_{b1}\omega_{b2}(h_{b1}\omega_{b2} - h_{b2}\omega_{b1})/(\omega_{b2}^2 - \omega_{b1}^2) \quad (32)$$

$$p_2 = 2(h_{b2}\omega_{b2} - h_{b1}\omega_{b1})/(\omega_{b2}^2 - \omega_{b1}^2) \quad (33)$$

Where p_1 and p_2 are the damping ratio coefficients. ω_{b1} and ω_{b2} , respectively, denote the first and second natural circular frequencies of the rigid-frame viaduct; h_{b1} and h_{b2} are the damping constants corresponding to ω_{b1} and ω_{b2} respectively.

Assuming the total number of cars as h , the external force vector \mathbf{f}_b can be represented as follows

$$\mathbf{f}_b = \sum_{j=1}^h \sum_{l=1}^2 \sum_{k=1}^2 \sum_{m=1}^2 \{\Psi_{jylkm}(t) P_{jylkm}(t) + \Psi_{jzlk m}(t) P_{jzlk m}(t)\} \quad (34)$$

Where $P_{jylkm}(t)$, $P_{jzlk m}(t)$ and $\Psi_{jylkm}(t)$, $\Psi_{jzlk m}(t)$ are the wheel loads of the train and the distribution vectors respectively, which are described above in the high-speed train formulization.

The modal analysis technique is then applied to the rigid-frame viaduct system to simplify the calculation process (Kawatani *et al.* 2006).

3.3 Coupled equations of the TBI system

Coupled vibration responses of the TBI system are analyzed by taking train-bridge interaction into consideration based on the developed computer program. The vibration behavior of the TBI system is a complex coupled time-varying vibration problem. This problem is generally solved by a numerical simulation based on a vibration interaction model for the whole TBI system. Theoretically, the analytical model is mainly composed of the high-speed train subsystem and the rigid-frame RC viaduct subsystem, each of them characterized by some vibration differential equations. Consequently, based on the above formulization, the coupled vibration differential equations of the TBI system can be expressed

$$\begin{bmatrix} \mathbf{M}_t & \mathbf{0} \\ \text{Sym.} & \mathbf{M}_b \end{bmatrix} \begin{Bmatrix} \ddot{\mathbf{w}}_t \\ \ddot{\mathbf{w}}_b \end{Bmatrix} + \begin{bmatrix} \mathbf{C}_t & \mathbf{C}_{bt} \\ \text{Sym.} & \mathbf{C}_b \end{bmatrix} \begin{Bmatrix} \dot{\mathbf{w}}_t \\ \dot{\mathbf{w}}_b \end{Bmatrix} + \begin{bmatrix} \mathbf{K}_t & \mathbf{K}_{bt} \\ \text{Sym.} & \mathbf{K}_b \end{bmatrix} \begin{Bmatrix} \mathbf{w}_t \\ \mathbf{w}_b \end{Bmatrix} = \begin{Bmatrix} \mathbf{F}_t \\ \mathbf{F}_b \end{Bmatrix} \quad (35)$$

Where \mathbf{M}_t , \mathbf{C}_t and \mathbf{K}_t denote the mass, damping and stiffness matrices of the high-speed train system respectively; \mathbf{M}_b , \mathbf{C}_b and \mathbf{K}_b denote the mass, damping and stiffness matrices of the rigid-frame RC viaduct system respectively; \mathbf{C}_{bt} , \mathbf{K}_{bt} and the symmetrical parts indicate the coupled components of the TBI system; \mathbf{w}_t and \mathbf{w}_b are the generalized displacement vectors respectively; \mathbf{F}_t and \mathbf{F}_b are the external force vectors of the TBI system, respectively.

Vibration reaction forces at the bottoms of piers cannot be determined accurately through modal analysis by means of calculating the shear forces at the ends of piers due to the Gibbs phenomenon. Thus, they can be calculated by using the influence value matrix of the reaction force

$$\mathbf{R}(t) = \mathbf{K}_R(\mathbf{P}_{vst} + \mathbf{P}_{vdy}) + \mathbf{K}_R\mathbf{P}_{sdy} \quad (36)$$

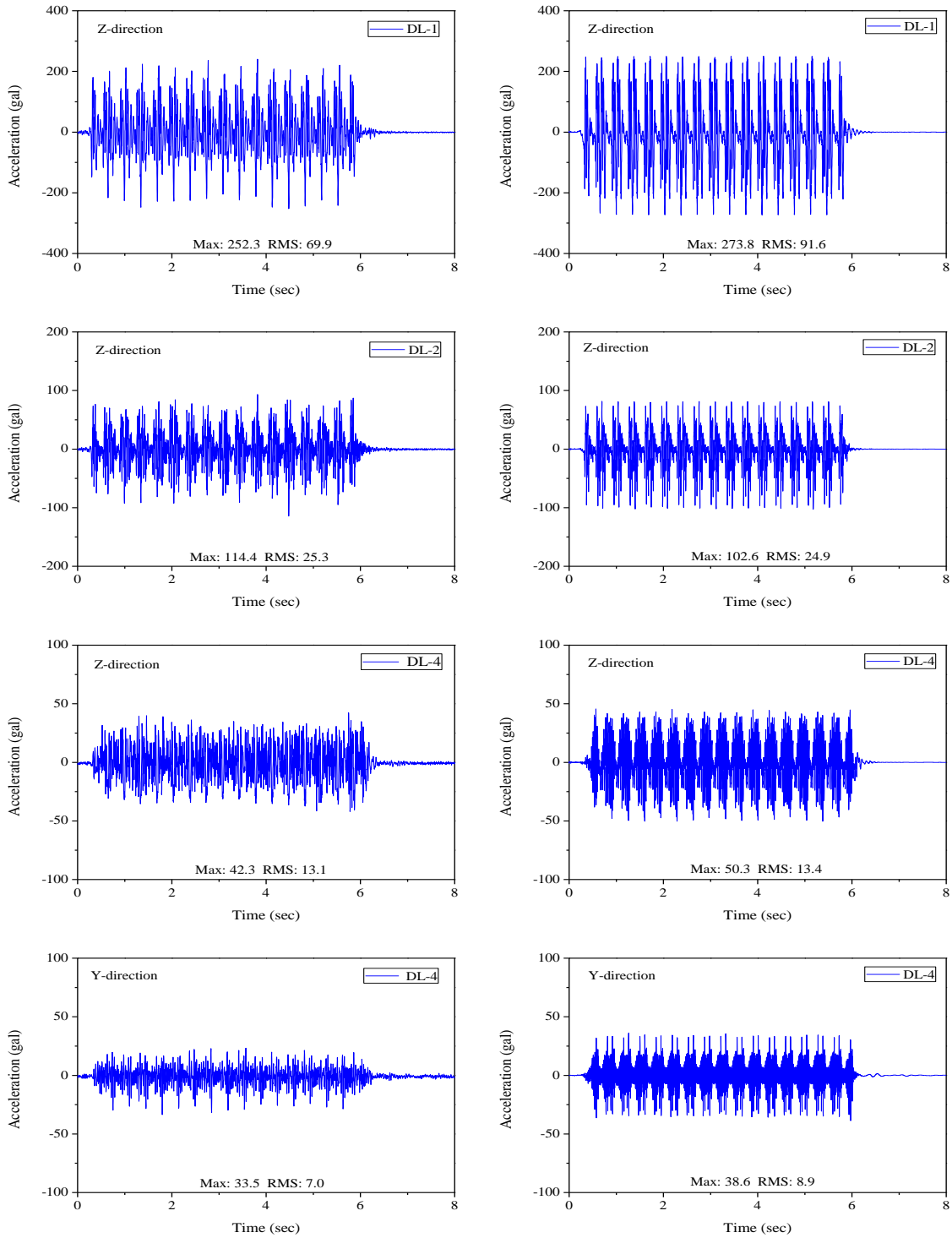
Where $\mathbf{R}(t)$ and \mathbf{K}_R denote the reaction force vector and the influence value matrix of the reaction force respectively; \mathbf{P}_{vst} , \mathbf{P}_{vdy} and \mathbf{P}_{sdy} denote the static and dynamic components of the wheel loads and the inertia forces of the rigid-frame RC viaduct nodes, respectively.

The Newmark- β method is utilized to solve the coupled vibration differential equations of the TBI system. Adopting 1/4 as the value of β , the vibration responses can be computed accurately with less than 1/1000 error for acceleration at each time step. In addition, the validity of the analytical procedure can be verified by comparing the analytical results with experimental observations. Considering the extremely high speed of the train, the integral time interval is set as 0.0005s.

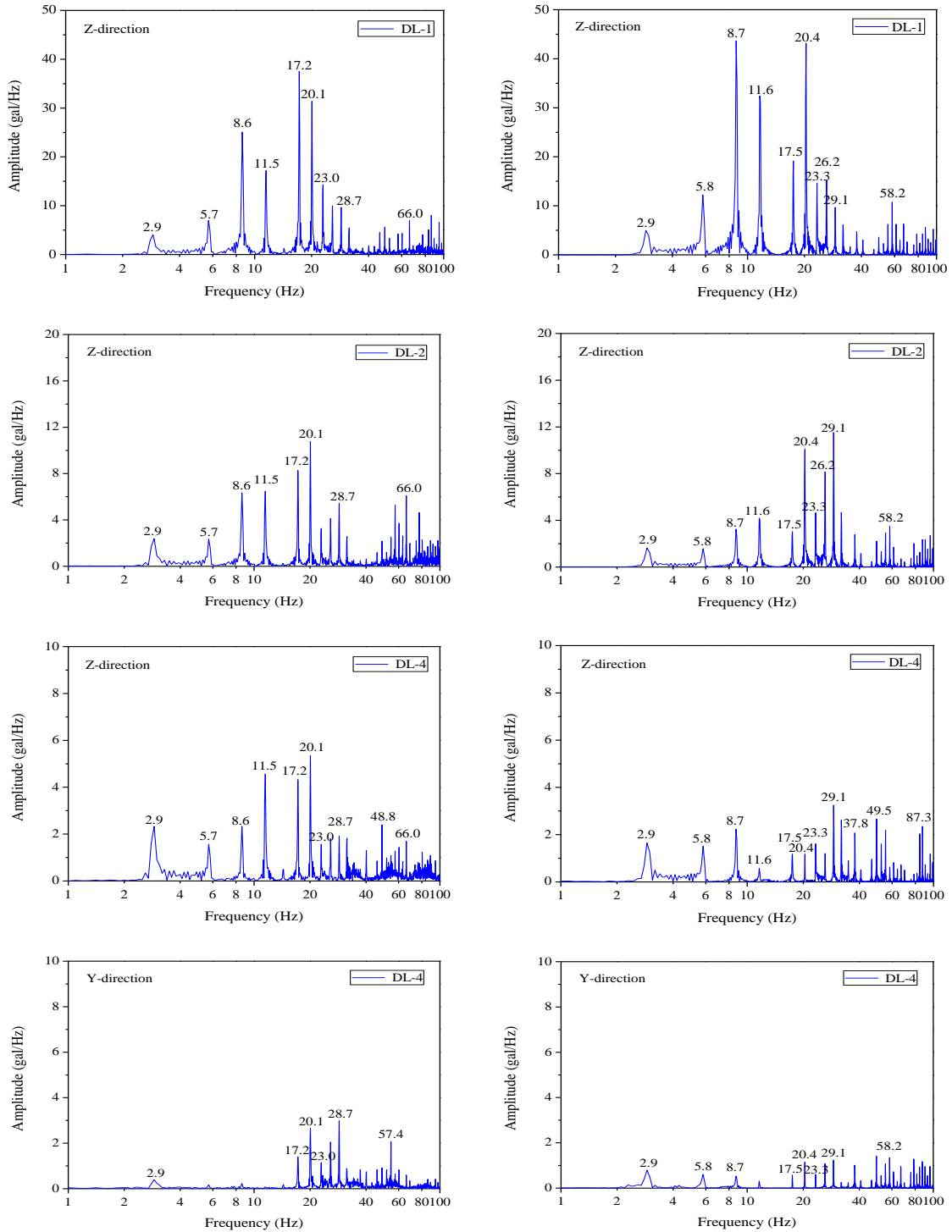
4. Vibration response analysis

The rigid-frame RC viaduct model and the computer program for simulating dynamic responses of the TBI system are demonstrated in this study so as to verify the validity through comparison with experimental results. Then, the dynamic responses of the viaducts including accelerations and displacements are clarified by means of 3D numerical analysis in both vertical and lateral directions. The reaction forces at the pier bottoms are also calculated for further ground vibration analysis as input excitation forces.

To confirm the validity of the viaduct model, the eigenvalue analysis was performed, that of vibration modes and more detailed information can be found in the reference (Kawatani *et al.* 2006). The predominant frequency 2.2 Hz of the horizontal natural mode was consistent with the value 2.2 Hz from the field testing. Consequently, the validation of the rigid-frame RC viaduct model can be confirmed. For the field measurement, the vibration testing was conducted at one viaduct of the Shinkansen line. While the 300 Series Shinkansen train composed of sixteen cars was running through the viaducts at the speed of 262 km/h. The acceleration time histories of the viaducts were recorded after being processed by signal amplifiers. The sampling frequency was 512 Hz. The measured points of the bridge vibration are displayed in Fig. 3 such as DL-1, DL-2 and DL-4, which, respectively, are the hanging part, on top of both the first and the third piers of the middle viaduct in the down line (DL), with respect to the direction that the high-speed train runs towards. Regarding the numerical analysis, the predominant frequencies of the vertical bending natural mode and the torsional mode are about 11.9 Hz and 13.9 Hz, respectively. The



(a) Experiment (b) Analysis
 Fig. 5 Time histories of acceleration responses of rigid-frame RC viaducts



(a) Experiment

(b) Analysis

Fig. 6 Fourier spectra of acceleration responses of rigid-frame RC viaducts

highest frequency taken into account in the analysis is about 102 Hz corresponding to the 277th natural mode. The predominant frequencies of the rail mode are larger than 200 Hz, but it is considered that the influence of the rail vibration on the structures can be neglected. Thus, the higher frequency components of the bridge vibration should be sufficiently taken into consideration and the highest frequency interested in environmental vibration problems is less than 100 Hz. Therefore, the highest frequency taken into account in the analysis is set as 100 Hz. In general, it is difficult to reproduce the completely accurate dynamic responses of the viaduct based on the numerical analysis because of uncertainties in modeling either the high-speed train or the rigid-frame RC viaduct. However, it is sufficient in most cases if the amplitudes and main dynamic components can be expressed for the actual discussion in the field of the civil engineering.

4.1 Acceleration response

4.1.1 Time history and Fourier spectrum

The analytical and experimental time histories and Fourier spectra of vibration acceleration responses of the viaducts in both vertical and lateral directions at the speed of 262 km/h are displayed in Figs. 5 and 6, respectively. Their maximum (Max) accelerations and root-mean-square (RMS) values are also indicated in the figures. The computation was carried out with the developed analytical program based on the conditions of the field measurement and the actual properties of the rigid-frame RC viaduct and the high-speed train.

It can be seen in Fig. 5 that each time history consists of seventeen blocks of vibration among these results because the high-speed train has sixteen cars altogether and each block of vibration corresponds to each train bogey passing the viaducts. The acceleration responses in the vertical are much larger than those in the lateral because the vertical excitation includes moving multi-DOFs vibration system and vertical irregularity but the lateral excitation includes lateral irregularity. This demonstrates that the vertical vibration has a big influence on the vibration responses of the viaducts. For the vertical direction, the acceleration responses indicate the tendency of DL-1>DL-2>DL-4. This proves that the vibration influences at the hanging parts are larger than those at other parts of the viaducts. Because the hanging parts of the rigid-frame RC viaducts are connected with neighboring ones by rails and ballast in the actual structure, but only the rails' connecting effect can be incorporated into the analysis. Perhaps for this reason, high-speed train-induced vibrations

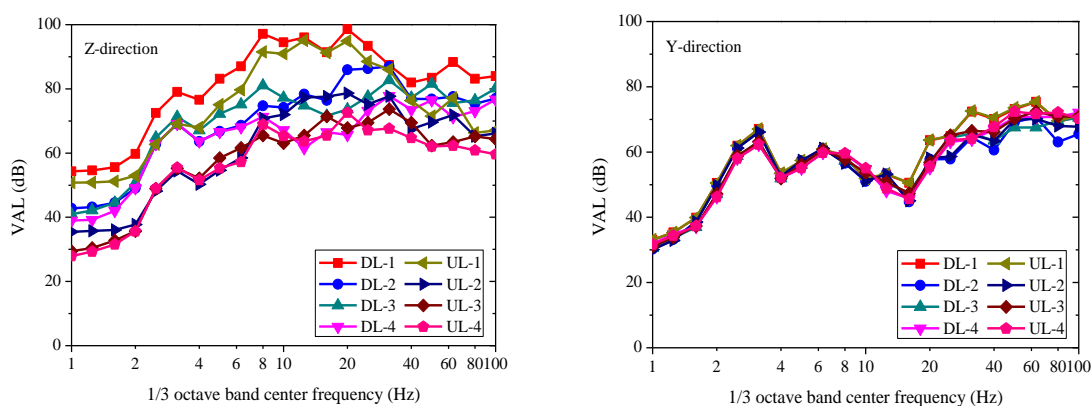


Fig. 7 1/3 octave band spectra of vertical and lateral vibration responses

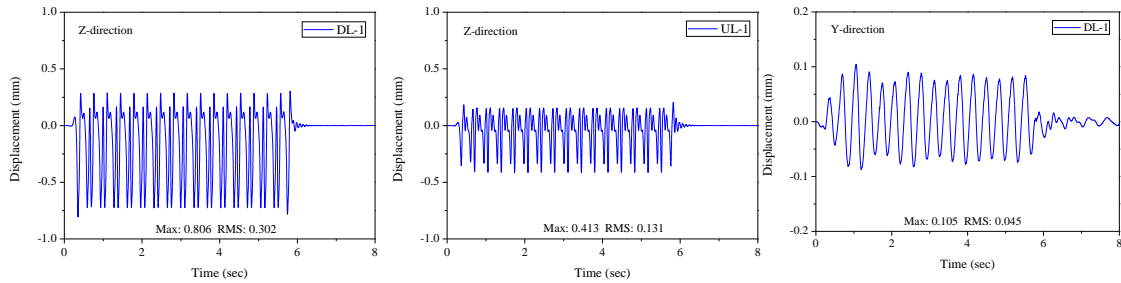


Fig. 8 Time histories of displacement responses of rigid-frame RC viaducts

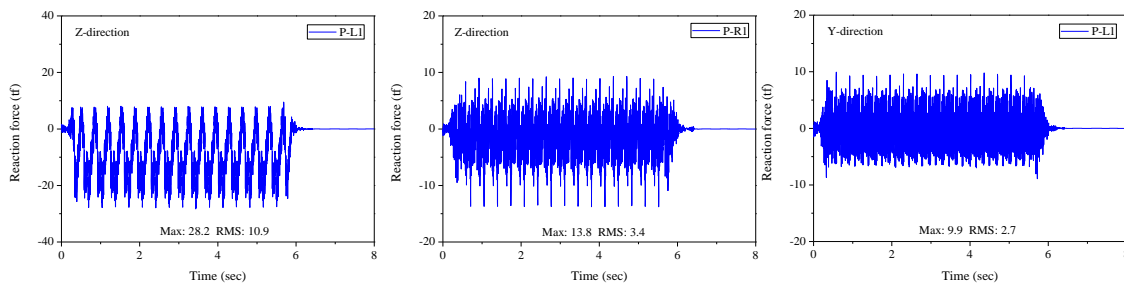


Fig. 9 Time histories of vibration reaction forces at the pier bottoms

are predominant at lower frequencies and analytical acceleration responses display larger amplitudes than the experimental ones at the hanging parts. The maximum probability of error of analytical results is no more than 18.9% in comparison with experimental results.

It is observed from Fig. 6 that the frequency components of analytical results are quite similar to those of experimental results but there are some differences at DL-4 in the lateral direction below 20Hz. Because the vertical vibrations are caused by the moving multi-DOFs vibration system and vertical irregularity but the lateral vibrations are caused by lateral irregularity. The stochastic process time samples are adopted for the track irregularities which are different from the actual track irregularities with respect to field measurement. The Fourier spectra show distinct peaks of vibration around 10 Hz and 20 Hz which are determined by the wavelength of the repeated one car length 25 m. The primary frequency 2.9 Hz is the same between analytical and experimental results and the higher frequencies are integral multiples of 2.9 Hz.

The analytical results demonstrate the relative consistency with experimental observations in three aspects: amplitudes, distribution tendencies and frequency components. Therefore, the validity of the proposed analytical procedure of the TBI system can be verified. The analysis system can be applied to represent the train-induced vibration behaviors of the bridge and the high-speed train due to take into account the TBI, but further improvement is needed for more accurate research results.

4.1.2 One-third octave band spectrum

The 1/3 octave band spectra of vibration responses of the viaducts in both vertical and lateral directions at the speed of 262 km/h are indicated in Fig. 7. It is seen that the same primary frequency components of bridge vibrations at the center frequencies 3.15 Hz in both vertical and lateral directions due to the effect of the periodic axle load with respect to the speed of the train.

However, there are some differences between the vertical and lateral directions. For instance, the vertical VAL is larger in the low frequency band (8~20 Hz) while the lateral VAL is larger in the high frequency band (31.5-63 Hz). The vertical VAL of the down line is larger than that of the up line but the lateral VAL is very close at different observation points. That is because the vertical excitation is mainly the multi-DOFs vibration system on the down line but the lateral excitation is mainly lateral irregularity which can easily cause the higher frequency vibration. The other probable reason is that the lateral forces of the wheel-rail in the left rail are the same as those in the right rail due to the application of the same lateral irregularity. It is reconfirmed that the vertical vibration intensity is stronger than that in the lateral direction.

4.2 Displacement response

Displayed in Fig. 8 are the displacement time histories of the rigid-frame RC viaducts in both vertical and lateral directions at the speed of 262km/h with the Max and RMS values also indicated. The curves in the figure demonstrate that the vertical displacement is much larger than that in the lateral direction. Each vertical time history has 32 minus peaks because the high-speed train has a total of 32 wheel-sets then each minus peak corresponds to each wheel-set passing the viaducts and lateral time history is also changed periodically. The displacement response of the down line is much larger than that of the up line in the vertical direction but the lateral displacement response is similar for different observation points.

4.3 Vibration reaction force

As shown in Fig. 9, the time histories of vibration reaction forces at the pier bottoms together with their Max and RMS values in both vertical and lateral directions at the speed of 262 km/h are calculated using the influence value matrix of the reaction forces. On the one hand, the vertical reaction forces of the pier bottoms on the left side are much stronger than those on the right side because the high-speed train is assumed to run along the left side of the viaducts. On the other hand, the vibration reaction forces on the left and right sides in the lateral direction display similar amplitudes. Furthermore, these vibration reaction forces obtained here can be used as input external excitations in further analyses of ground vibration problems. They can also imply how much they affect the ground vibration.

4.4 Vibration influence of rigid-frame RC viaducts with train speeds

The train speed is the most crucial factor affecting the dynamic responses in the railway bridges. With the speed improvement of high-speed trains, dynamic characteristics of the TBI system become more and more important. It is necessary to investigate the dynamic effects of rigid-frame RC viaducts under different train speeds for the purposes of the safe running, comfortable riding and environmental vibration improvement. Thus, the dynamic effects of the viaducts within the train speed range of 90-360km/h in the vertical direction are investigated based on maximum acceleration, frequency component, maximum displacement, maximum reaction force and DAF of the rigid-frame RC viaducts and the made observations are displayed in Fig. 10. The investigation is carried out based on the fact that the vertical vibration is much larger than the lateral vibration and the lateral vibration influence for different observation points is similar based on above vibration response analysis.

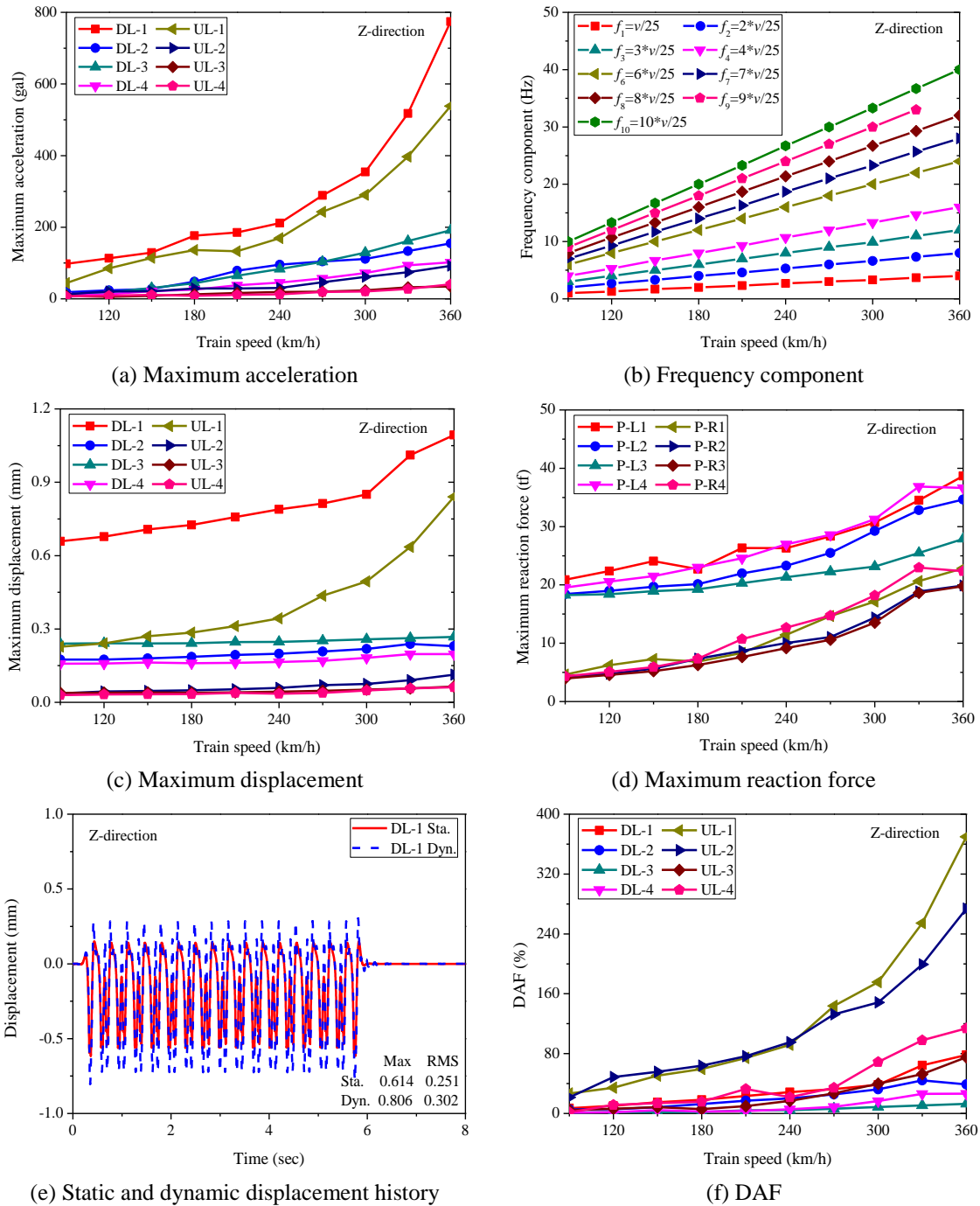


Fig. 10 Vibration influence of rigid-frame RC viaducts with train speeds in the vertical direction

4.4.1 Maximum acceleration

It is observed in Fig. 10(a) that the maximum accelerations of the down line and up line

become larger with increasing train speeds for the overall trend in the vertical direction. The vibration responses in the down line are larger than those in the up line because it is assumed that the high-speed train is running on the down line. The dynamic responses of hanging parts are much larger than those of other parts. It is found that the dynamic responses of the hanging parts are predominated for the whole vibration responses. It is useful to mitigate the viaduct vibration through reinforcing the hanging part. Regarding different observation points, the vibration behaviors are similar in trend but different in magnitude due to the different position in rigid-frame RC viaducts.

4.4.2 Frequency component

Vibration frequency components are determined by the wavelength of the repeated one car length (L) and the distance between the two wheel-sets ($2\lambda_{x2}$). From the wavelengths of all the possible combinations of wheel-sets and the number of repeated passing times for each high-speed train, it is found that the wavelength of one car length has the highest number of appearances. If the high-speed train passes the viaducts with a speed of v (m/s), the relationship between the vibration frequency component and the train velocity can be calculated as follows

$$f_1 = v/L = v \text{ (m/s)}/25m \quad (37)$$

$$f_{10} = v/2\lambda_{x2} = v \text{ (m/s)}/2.5m = 10f_1 \quad (38)$$

The higher vibration frequencies are integral multiples of the primary vibration frequency f_1 . In this study, f_1 is 2.9 Hz at the train speed of 262 km/h, and the integral relation is also shown in Fig. 6, which agrees well with the dominant frequency in the measurements by Miyashita *et al.* (2007). Simultaneously, the vibration frequency property is also indicated for another train speeds as shown in Fig. 10(b). Therefore, the analytical results can be used to represent the frequency properties of the high-speed train-induced vibrations.

4.4.3 Maximum displacement

As displayed in Fig. 10(c), the maximum displacements of the viaducts vary with train speeds and different observation points. The maximum displacements of hanging parts are much larger than those of the other parts and vary significantly with increasing the train speeds. That is because the hanging parts are modeled as the cantilever beams with weak restraints. It is an effective way to enhance the rigidity and reduce the vibrations of the rigid-frame RC viaducts through reinforcing the hanging parts. It is also indicated that the maximum displacements in the down line are larger than those in the up line.

4.4.4 Maximum reaction force

It can be seen from Fig. 10(d) that the maximum reaction forces at the pier bottoms are becoming larger and larger with the increase in the train velocity. It is verified once more that the vertical maximum reaction forces along the left side are larger than the counterpart of the right side because the high-speed train is assumed to run along the left side of rigid-frame RC viaducts. In particular, the amplitude at P-L1 is somewhat larger than that at P-L2. The probable reason is that maximum acceleration responses engender a larger inertia force appears at the hanging part of the viaducts in Fig. 5. Furthermore, these obtained reaction forces can be as input external excitation of the ground vibration analysis to investigate further the influence of train-induced ground vibration.

4.4.5 Dynamic amplification factor

The dynamic behaviors of rigid-frame RC viaducts are also explained in terms of the dynamic amplification factor, which is defined as Eq. (39).

$$DAF(\%) = (R_{Dyn.} - R_{Sta.})/R_{Sta.} \times 100\% \quad (39)$$

Where $R_{Dyn.}$ and $R_{Sta.}$ denote the absolute maximum dynamic response and static response of the viaducts, respectively. The dynamic and static displacement histories of the hanging part DL-1 at the train speed 262 km/h are displayed in Fig. 10(e). The DAF of DL-1 is 31.3%.

As shown in Fig. 10(f), the rule about the DAFs of rigid-frame RC viaducts has increased trend with increasing of train velocity for the different observation points in the vertical direction. But there are some differences between the increasing rate of down line and that of up line. It is found that the DAFs of down line are smaller than those of up line especially at the hanging parts. This could be attributed to the fact that the higher the static response generated, the smaller DAF is obtained as in Eq. (39).

5. Conclusions

The dynamic characteristics of rigid-frame RC viaducts in both vertical and lateral directions induced by running high-speed trains under simulated track irregularities are actively investigated in this study based on detailed 3D numerical analysis.

- The analytical model and three-dimensional numerical analysis algorithm of the TBI system are established and verified to reflect effectively the vibration behaviors of the viaducts. The analytical results are consistent with the experimental observations for the acceleration response curves, amplitudes, distribution tendencies and frequency components.

- High-speed train-induced dynamic characteristics of the rigid-frame RC viaducts in both vertical and lateral directions are clarified from three aspects: acceleration responses, displacement responses and vibration reaction forces of pier bottoms. Vibration effect of the viaducts in the vertical direction is much more serious than that in the lateral direction. It is verified that the hanging part is the most important part of the viaduct in which the high-speed train can induce the serious vibration influence.

- Frequency characteristics are further clarified based on Fourier spectral analysis and 1/3 octave band spectral analysis. It is observed that frequency components are basically similar for different observation points or directions. The corresponding amplitudes are different to some extents. The vertical vibration is induced by the multi-DOF vibration system and vertical irregularity while the lateral vibration is mainly caused by lateral irregularity, which can easily cause the higher frequency vibration.

- It is verified that train-induced vibration frequency of the viaducts is mainly dependent on the train speed in relation to the car length, the distance of centers of bogies and axes by means of the 3D numerical analysis. These frequency components are integer multiples of the primary frequency component. Therefore, it is beneficial to avoid the viaduct resonance by adjusting the train velocity based on the natural frequencies of the viaduct.

- Dynamic effects of rigid-frame RC viaducts within the train speed range of 90-360km/h have been discussed in detail from five aspects. It is reconfirmed that the train velocity is the most important impact factor to influence the train-induced vibration responses. The dynamic responses of the viaducts increase with the increasing train velocity especially at the hanging parts. It is seen

that the DAFs of the down line are smaller than those of the up line while the DAFs of the hanging parts are much larger than those of other parts of the corresponding line. Thus, the reinforcement of the hanging parts can be as an effective countermeasure to reinforce the 50-year old rigid-frame RC viaduct and mitigate the train-induced vibration.

- This study is significant to provide not only a simulation and evaluation approach for the train-induced vibration upon the rigid-frame RC viaducts but also beneficial instruction on the vibration mitigation of the high-speed railway.

Acknowledgements

This work was supported by fund from the National Natural Science Foundation of China (No: 51178365) and financially supported by self-determined and innovative research funds of WUT (No: 2010-YB-14).

References

- Chen, B. and Xu, Y.L. (2007), "A new damage index for detecting sudden change of structural stiffness", *Struct. Eng. Mech.*, **26**(3), 315-341.
- Chen, G. and Zhai, W.M. (1999), "Numerical simulation of the stochastic process of railway track irregularities", *J. Southwest Jiaotong Univ.*, **34**(2), 138-142. (in Chinese)
- Dinh, V.N., Kim, K.D. and Warnitchai, P. (2009), "Dynamic analysis of three-dimensional bridge-high-speed train interactions using a wheel-rail contact model", *Eng. Struct.*, **31**(12), 3090-3106.
- Fřyba, L. (1996), *Dynamics of Railway Bridges*, Thomas Telford Ltd., London, UK.
- Garinei, A. and Risitano, G. (2008), "Vibrations of railway bridges for high speed trains under moving loads varying in time", *Eng. Struct.*, **30**(3), 724-732.
- Guo, W.W., Xia, H., De Roeck, G. and Liu, K. (2012), "Integral model for train-track-bridge interaction on the Sesia viaduct: dynamic simulation and critical assessment", *Comput. Struct.*, **112-113**, 205-216.
- He, X.W., Kawatani, M. and Nishiyama, S. (2010), "An analytical approach to train-induced site vibration around Shinkansen viaducts", *Struct. Infr. Eng.*, **6**(6), 689-701.
- Ju, S.H., Lin, H.T. and Chen, T.K. (2007), "Studying characteristics of train-induced ground vibrations adjacent to an elevated railway by field experiments", *J. Geotech. Geoenviron. Eng.*, **133**(10), 1302-1307.
- Kawatani, M., He, X.W., Shiraga, R., Seki, M., Nishiyama, S. and Yoshida, K. (2006), "Dynamic response analysis of elevated railway bridges due to Shinkansen trains", *J. Struct. Earthq. Eng.*, JSCE, **62**(3), 509-519. (in Japanese)
- Kwark, J.W., Choi, E.S., Kim, Y.J., Kim, B.S. and Kim, S.I. (2004), "Dynamic behavior of two-span continuous concrete bridges under moving high-speed train", *Comput. Struct.*, **82**(4-5), 463-474.
- Martínez-Rodrigo, M.D., Lavado, J. and Museros, P. (2010), "Transverse vibrations in existing railway bridges under resonant conditions: single-track versus double-track configurations", *Eng. Struct.*, **32**(7), 1861-1875.
- Matsuura, A. (1998), "Simulation for analyzing direct derailment limit of running vehicle on oscillating tracks", *J. Struct. Earthq. Eng.*, JSCE, **15**(1), 63-72.
- Miyashita, T., Ishii, H., Fujino, Y., Shoji, T. and Seki, M. (2007), "Understanding of high-speed train-induced local vibration of a railway steel bridge using laser measurement and its effect by train speed", *J. Struct. Mech. Earthq. Eng.*, JSCE, **63**(2), 35-47. (in Japanese)
- Nishimura, A. (1990), "A study on integrity assessment of railway rigid frame bridge", *RTRI Rep.*, **4**(9), 14-21. (in Japanese)
- Railway Technical Research Institute (RTRI) (1997), *Design Standard for Railway Structures (Foundation*

- and Soil Pressure Resistance Structures), Maruzen Co., Ltd., Tokyo, Japan. (in Japanese)
- Olmos, J.M. and Astiz, M.A. (2013), "Analysis of the lateral dynamic response of high pier viaducts under high-speed train travel", *Eng. Struct.*, **56**, 1384-1401.
- Rezvani, M.A., Vesali, F. and Eghbali, A. (2013), "Dynamic response of railway bridges traversed simultaneously by opposing moving trains", *Struct. Eng. Mech.*, **46**(5), 713-734.
- Su, D., Fujino, Y., Nagayama, T., Hernandez, Jr. J.Y. and Seki, M. (2010), "Vibration of reinforced concrete viaducts under high-speed train passage: measurement and prediction including train-viaduct interaction", *Struct. Infr. Eng.*, **6**(5), 621-633.
- Takemiya, H. and Bian, X.C. (2007), "Shinkansen high-speed train induced ground vibrations in view of viaduct-ground interaction", *Soil Dyn. Earthq. Eng.*, **27**(6), 506-520.
- Tanabe, M., Wakui, H., Matsumoto, N., Okuda, H., Sogabe, M. and Komiya, S. (2003), "Computational model of a Shinkansen train running on the railway structure and the industrial applications", *J. Mater. Proc. Tech.*, **140**(1-3), 705-710.
- Uno, M., Sogabe, M., Tanimura, Y. and Kanamori, M. (2007), "A study on dynamic response of the railway continuous girder by running high-speed train", *J. Struct. Eng.*, JSCE, **53A**, 67-76. (in Japanese)
- Wakui, H., Matsumoto, N., Matsuura, A. and Tanabe, M. (1995), "Dynamic interaction analysis for railway vehicles and structures", *J. Struct. Earthq. Eng.*, JSCE, No.513/ I -31, 129-138. (in Japanese)
- Xia, H., Deng, Y.S., Xia, C.Y., De Roeck, G., Qi, L. and Sun, L. (2013), "Dynamic analysis of coupled train - ladder track -elevated bridge system", *Struct. Eng. Mech.*, **47**(5), 661-678.
- Xia, H., De Roeck, G. and Goicolea, J.M. (2011), *Bridge Vibration and Controls: New Research*, Nova Science Publishers, New York, USA.
- Xia, H., Zhang, N. and Gao, R. (2005), "Experimental analysis of railway bridge under high-speed trains", *J. Sound Vib.*, **282**(2), 517-528.
- Xie, W.P. and Xu, W. (2012), "Vehicle-induced vibration responses of a rail box girder in Wuhan Station", *J. Vib. Shock*, **31**(8), 186-190. (in Chinese)
- Yang, Y.B. and Lin, C.W. (2005), "Vehicle-bridge interaction dynamics and potential applications", *J. Sound Vib.*, **284**(1-2), 205-226.
- Yang, Y.B., Yau, J.D. and Wu, Y.S. (2004), *Vehicle-Bridge Interaction Dynamics: With Applications to High-Speed Railways*, World Scientific, Singapore.
- Yokoyama, H., Yashiro, K., Kamohara, A. and Iwata, N. (2011), "Propagation characteristics of horizontal and vertical component of train-induced ground vibration", *RTRI Rep.*, **25**(11), 35-40.
- Zhai, W.M., Wang, S.L., Zhang, N., Gao, M.M., Xia, H., Cai, C.B. and Zhao, C.F. (2013a), "High-speed train-track-bridge dynamic interactions-Part I: theoretical model and numerical simulation", *Int. J. Rail Trans.*, **1**(1-2), 3-24.
- Zhai, W.M., Wang, S.L., Zhang, N., Gao, M.M., Xia, H., Cai, C.B. and Zhao, C.F. (2013b), "High-speed train-track-bridge dynamic interactions-Part II: experimental validation and engineering application", *Int. J. Rail Trans.*, **1**(1-2), 25-41.